Inhomogeneities in plastically deformed silicon single crystals. II. Deep-level transient spectroscopy investigations of *p*- and *n*-doped silicon

C. Kisielowski and E. R. Weber
Department of Materials Science and Mineral Engineering, University of California, Berkeley, California 94720
(Received 21 August 1990)

The deep-level transient spectroscopy (DLTS) spectra of *p*- and *n*-type silicon samples, which were plastically deformed in the temperature range $390\,^{\circ}\mathrm{C} \leq T_d \leq 800\,^{\circ}\mathrm{C}$ with different resolved shear stresses $8 \leq \tau \leq 200$ MPa, can be quantitatively related to the deformation-induced ESR spectra. Deformation-induced point defects are inhomogeneously distributed and produce dominant energy levels in the lower half of the band gap. A smaller amount of dislocation-related defects causes energy levels in the upper part and in the middle of the band gap. The deformation-induced defects compensate *p*- and *n*-type material. The DLTS linewidths can be simulated by the introduction of a broadening parameter δ, which describes deformation-induced disorder. From its dependence on the applied deformation stress (21.5 meV/GPa in *n*-type material) and the similarity of the value to the pressure derivative of the conduction-band edge, we conclude that part of the disorder is related to fluctuations of the band edges. Contributions of fluctuating Coulomb potentials and variations of the capture cross sections caused by compensation probably contribute to the broadening of the energy levels. Similarities to polycrystalline materials are discussed.

I. INTRODUCTION

In the preceding paper it was shown that plastic deformation of silicon introduces deep-level defects that are rather inhomogeneously distributed with respect to chemical dopants.[1] Most of the deformation-induced defects were attributed to ordinary deep point defects and only roughly a quarter of them could be related to the core of dislocations.[2] Thus, in contrast to extended defects such as dislocations which are expected to trap only a limited amount of charge because of Coulomb repulsion[3] the charge state of most deformation-induced defects can be changed by doping as long as the local defect density does not exceed the concentration of the chemical dopants.[1] If so, it should be possible to detect at least the same amount of defects by deep-level transient spectroscopy (DLTS) than by electron-spin resonance (ESR) because the change of their charge state is accompanied by a change from diamagnetism to paramagnetism (or vice versa).[1] Deviations from that expectation would indicate the presence of a Coulomb barrier against the capture of charge or a local exhaustion of electrons or holes disposed from the shallow dopants.

In order to relate the DLTS levels to certain ESR signals we varied the deformation parameters and used deformations in molecular hydrogen because both procedures are known to influence the ESR spectra of deformed silicon[4,5] and this could facilitate the relation.

Thus, the study is devoted to the question how to correlate DLTS and ESR spectra quantitatively whereas the determination of energy levels, capture cross sections, filling behavior, and other aspects will not be treated in detail, in particular, because we observed data which with minor differences agree with what has been published before.[6–15]

While performing the experiments it turned out that the DLTS spectra exhibit large line widths which depend on details of the deformation procedures and that our experiments give additional information on mechanisms contributing to the line broadening.

II. EXPERIMENT

Plastic deformation of the crystals was performed by static compression along [213] in the same manner as in Ref. 1. The material properties and the deformation conditions are listed in Tables I and II. The deformation temperature T_d and the resolved shear stress τ ($=\sigma \times S$; σ is the external stress and S is the Schmid factor equal to 0.467 for deformations along [213]) was varied between $390\,^{\circ}\mathrm{C} \leq T_d \leq 800\,^{\circ}\mathrm{C}$ and $8 \leq \tau \leq 200$ MPa; the plastic strain $\epsilon = \delta l / l$ reached 3%. In the case of low-temperature high-stress deformations the crystals were predeformed (see Table I) to increase the initial dislocation density to roughly 10^7 cm^{-2} which is necessary to avoid brittle fracture.

Most of the experiments were done with the initially uncompensated materials *A* (*n*-type doped with phosphorous $n = N_{cd} = [\mathrm{P}]$) and *C* (*p*-type doped with boron $p = N_{ca} = [\mathrm{B}]$) to investigate the deformation-induced defects in the lower part of the band gap (N_t^p) and in its upper part (N_t^n).

After the main deformation slices of ≈ 400 μm thickness were cut parallel to the (011) planes, thus, the Burgers vector $a/2$ [011] (a is the lattice constant) of the main slip system [011], (1$\underline{1}$1) was perpendicular to the plane on which Schottky contacts were formed by evaporation of Au on *n*-type silicon and of Al on *p*-type silicon. The Ohmic contacts were produced on the back side of the slices by evaporation of Au on *p*-type silicon and by putting on a GaIn alloy on *n*-type samples.

The diodes were characterized by $I(U)$ and $C(U)$ mea-

TABLE I. A listing of low-temperature $T_d \leq 650$ °C deformed samples: FZ floating-zone Si with a grown-in dislocation density of $\approx 10^4$ cm^{-2}. Initial P or B doping of the materials: *A*, $[n]=4.4\times10^{15}$ cm^{-3}; *B*, $[n]=4\times10^{17}$ cm^{-3}; *C*, $[p]=3.2\times10^{16}$ cm^{-3}; *D*, $[p]=4.8\times10^{17}$ cm^{-3}; *E*, $[p]=1\times10^{15}$ cm^{-3}; T_d is the deformation temperature. τ is the resolved shear stress. ϵ is the plastic strain ($\delta l/l$ in %). $N_t^{n,p}$ is the trap concentration determined by TSCAP and DLTS (*D* line). *F* is the forming gas: 8% H_2+92% N_2. Concentrations are given in units of 10^{14} cm^{-3}.

Sample	T_d (°C)	τ (MPa)	ϵ (%)	$N_t^{n,p}$ TSCAP	$N_t^{n,p}$ *D* line	Gas ambient
*A*1	800	12	2.5	3.8	≤0.1	*F*
*A*2	650	30	2.8	2–6	5–8	*F*
*A*3	650	30	3.8	≤2	≈9	*F*
*A*4	650	90	1.3	2.2	5	*F*
*A*5	650	150	1.7	compensated		*F*
*A*6	550	30	2.9	4.5	4	*F*
*A*7[a]	550	90	2.1	≤10	≈10	*F*
*A*8[a]	550	150	1.8	4.2	4	*F*
*A*9[a]	420	150	1.4	4.0	≤1	*F*
*A*10[a]	390	200	0.8	5.0	≤1	*F*
*B*1	650	30	2.8	≤8		Ar
*C*1	800	12	3.0	6.5		*F*
*C*2	650	30	2.7	31		*F*
*C*3	650	30	2.7	20		Ar
*C*4	650	150	2.3	16		*F*
*C*5[a]	550	150	1.9	24		*F*
*C*6[a]	420	150	1.4	18		*F*
*D*1	650	30	3.0	27		Ar
*E*1	650	30	1.0	≈9		Ar

[a]Denotes samples predeformed at 800 °C. $\tau=12$ MPa, $\epsilon=0.7\%$.

surements to control the leakage current and to determine the effective free-carrier concentration $[n_e]$, $[p_e]$ being present after deformation as well as the built-in potential U_0.

Thermally stimulated capacitance (TSCAP) (Ref. 16) measurements were used to study the temperature dependence of the junction capacitance C for a total potential $U_1=U_r+U_0$ (U_r is the external reverse bias) and to determine the total concentration of the traps. For this purpose the samples were cooled with $U_r<0$ *V* from room temperature to 100–80 K, where U_r was removed for 1 s up to half an hour before the bias was reinstalled and the temperature increased. The rate of temperature change was approximately 5 K/min. From the capacitance drop at low temperature ΔC the trap density was determined by[16]

TABLE II. High-temperature-deformed and hydrogen-treated samples. Same symbols as in Table I; P doping of material *F*: $[n]=5\times10^{14}$ cm^{-3}; t_a and T_a are the annealing time and temperature, respectively. Sample *C*7 was (1) predeformed, (2) annealed, and (3) main deformed. Concentrations are given in units of 10^{14} cm^{-3}.

Sample	T_d (°C)	τ (MPa)	ϵ (%)	$N_t^{n,p}$ (TSCAP)	Gas ambient
*F*1	800	8	1.6	0.28	Ar
*F*1*T*	part of *F*1	$t_a=16$ h at $T_a=800$ °C		0.06	Ar
*F*2	800	8	1.6	0.98	H_2
*F*2*T*	part of *F*2	$t_a=16$ h at $T_a=800$ °C		0.07	H_2
*E*2	800	8	1.6	0.67	Ar
*E*2*T*	part of *E*2	$t_a=16$ h at $T_a=800$ °C		0.13	Ar
*E*3	800	8	1.6	1.35	H_2
*E*3*T*	part of *E*3	$t_a=1$ h at $T_a=800$ °C		0.16	H_2
*C*7(1)	800	8	1.6		H_2
*C*7(2)	$T_a=800$ °C	$t_a=16$ h			H_2
*C*7(3)	650	30	2.7	see Table IV	H_2

$$\Delta C/C \approx 0.5 N_t^n/n_e \quad (1)$$

(equations are given for n-type material and can be applied to p-type material by substitution of the appropriate quantities, N_t^p and p_e in this case).

From measurements of the $I(U)$ curve using a forward bias a resistance R in series with the junction was detected in several samples which falsifies the measured capacitances $\Delta C'$ and C' and needs to be corrected by[17]

$$C' = C/(1+R^2C^2\Omega^2)$$

and (2)

$$(\Delta C'/C')/(\Delta C/C) = (1-R^2C^2\Omega^2)/(1+R^2C^2\Omega^2)$$

with $\Omega = 1$ MHz being the frequency of the ac voltage (10 mV) of the capacitance meter.

Several DLTS spectrometers were used. Most of the experiments were performed with a computer controlled and modified HP 4240A capacitance meter[18] in the temperature range $80 \le T \le 350$ K which was also used for TSCAP and $C(U)$ measurements. The system was programmed to sample the capacitance transient at up to eight discrete time points from the interval 0.15–240 ms after each pulse and the time points were chosen to simulate a boxcar analyzer with $t_2/t_1 = 4$ (or 5). By appropriate combination of the time points up to 6 DLTS spectra were recorded with one temperature scan and the emission rates e_n (e_p for p-type materials) are given by $e_n = \ln(t_2/t_1)/(t_2-t_1)$.[19]

Some of the samples were investigated with the DLTS system used in Ref. 12 in order to reproduce the results of the previous DLTS study of deformed materials. For measurements down to ≈ 20 K another system was employed.[20]

From the DLTS spectra the defect concentration can be determined by[21]

$$\frac{\Delta C}{C} = -\frac{N_t}{2n_e}\frac{(W_1-\alpha)^2-(W_0-\alpha)^2}{W_1^2}\exp(-e_n t) \quad (3)$$

with W_0, W_1 being the depletion widths for $U = U_0$ and $U = U_1$, respectively, $\alpha = [2\epsilon_0(E_F - E_t)/e^2 n_e]$, e is the elementary charge, N_t is the trap concentration at the energy E_t, and E_F is the Fermi energy.

Since $U_1 > U_0$ ($U_1 = 4$–7 V and $U_0 \approx 0.8$ V) in most experiments, Eq. (3) reduces to

$$\Delta C/C \approx -\frac{N_t}{2n_e}\exp(-e_n t) . \quad (4)$$

However, in the deformed samples the broadening of the DLTS lines requires additional corrections as pointed out by Omling *et al.*[12] and Omling, Samuelson, and Grimmeiss.[22] In this case the capacitance transient is nonexponential and neglecting a possible temperature dependence and broadening of the capture cross section it is given by[23]

$$C(t) = C_0/\delta(2\pi)^{1/2}\int_0^{E_g} dE \exp[(E-E_t)^2/2\delta^2 - e_n t] \quad (5)$$

with

$$e_n = AT^2\exp(-E/kT) ,$$

where A is related to the capture cross section[23] of the defect. Thus, a broadened DLTS line needs to be simulated by use of Eq. (5) and in this case the determination of the defect concentration depends on the DLTS line amplitude and its width.[22] The concentrations of the D line given in this paper involve these corrections. In the case of resistances being present in series with the junctions the capacitances were corrected by Eq. (2).

III. RESULTS AND DISCUSSION

A. $C(U)$ and TSCAP measurements

Figure 1 shows the temperature dependence of the effective carrier concentration (n_e,p_e) as determined from $1/C^2(U)$ plots measured between 80 K and room temperature. The initial doping level (n or p) of the undeformed samples is marked by arrows. It can be seen that plastic deformation reduces the initial doping in n- and p-type material. Even close to room temperature the initial doping level was not reached which indicates the formation of deep deformation-induced defects.

Measurements on different slices cut from the same sample reveal that the data scattered up to a factor of 2 as indicated for sample $A2$ in Fig. 1. This gives an estimation of the experimental uncertainty. Most likely it is caused by the inhomogenous distributions of the defects even if the samples are cut from the most homo-

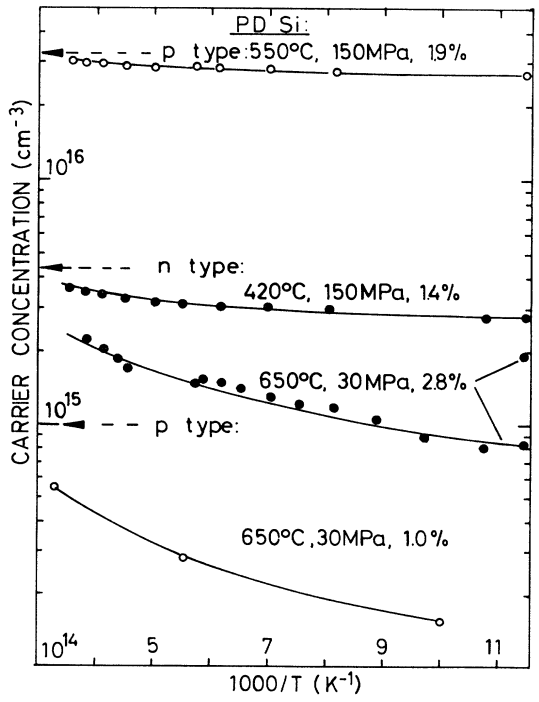

FIG. 1. Temperature dependence of the free-carrier concentration as determined from $1/C^2(U)$ measurements. Samples $C5$, $A9$, $A2$ (two measurements of different slices), and $E1$. Samples are labeled in Tables I and II. The arrows mark the initial doping of the materials.

geneous central part of the deformed crystals or by uncertainties in the determination of the Schottky contact area.

Since the defect concentration increases linearly with the plastic strain[24] for constant T_d and τ the concentration of deep defects, ϵ can be estimated from the low-doped p- and n-type samples $A2$ and $E1$ by subtraction of n_e (or p_e) from n (or p) at low temperature because the deep deformation-induced defects must be charged by compensating the shallow dopants at low temperature. Thus, $N_t/\epsilon \approx [n - n_e(100\ \text{K})]/\epsilon = (0.89-1.28)\times 10^{15}$ defects $\text{cm}^{-3}\,\epsilon^{-1}$ and $N_t/\epsilon \approx [p - p_e(100\ \text{K})]/\epsilon = 0.85 \times 10^{15}$ defects $\text{cm}^{-3}\,\epsilon^{-1}$ [in material C this value can only roughly be estimated to $\leq 2\times 10^{15}$ defects $\text{cm}^{-3}\,\epsilon^{-1}$ because of the high initial doping; numerical values for the strain used in this paper are $\epsilon = (\delta l/l)\%$]. Since these numbers are equal within the experimental errors the estimation indicates that plastic deformation introduces amphoteric defects which are donorlike in p-type material and acceptorlike in n-type material. This result was used in Ref. 1. In addition Fig. 1 shows that the compensation $K_n = N_t/N_{cd}$ ($K_p = N_t/N_{ca}$ for p-type material) is large in the low-doped materials. It reaches values of 0.85.

Figures 2(a) and 2(b) show typical examples for TSCAP measurements of samples deformed at $T_d = 650\,^\circ\text{C}$. Figure 2(c) shows a measurement of a high-temperature deformed and annealed n-type sample and Fig. 2(d) shows a p-type sample which was high temperature deformed only. The strong drop of the $C(T)$ curve ($\approx 0.5\times 10^{-10}$ F) with decreasing temperature in Fig. 2(a) is a result of the compensation in this sample. In Fig. 2(b) this drop is influenced by a resistance in series with the junction and it is small in Figs. 2(d) and 2(c). It can be seen that no single steps could be observed in the p-type material indicating a "continous" distribution of deep defects; high-temperature annealing did not change the situation. In contrast, in the n-type material different contributions labeled B, C, and D could be resolved. However, the C level could only be well identified in a high-temperature deformed and annealed sample [Fig. 2(c)].

From the change of the capacitance at low temperature ΔC the total concentration of deep traps in the samples was determined [Eqs. (1) and (2) if necessary] and these values are listed in Tables I and II. From the tables it can be seen that the concentration of deep levels in the upper part of the band gap (n-type material) is smaller than in its lower part (p-type material) for $T_d \leq 650\,^\circ\text{C}$ but this difference decreases with increasing deformation temperature (Table II).

Changing the pulse length from 1 s to half an hour did not affect ΔC and this proves that all traps could be filled by application of 1-s pulses. This holds particularly for the D level [Fig. 2(a)] even if the temperature for the filling pulse was varied from 80 to 220 K. It demonstrates that from TSCAP mesurements one must con-

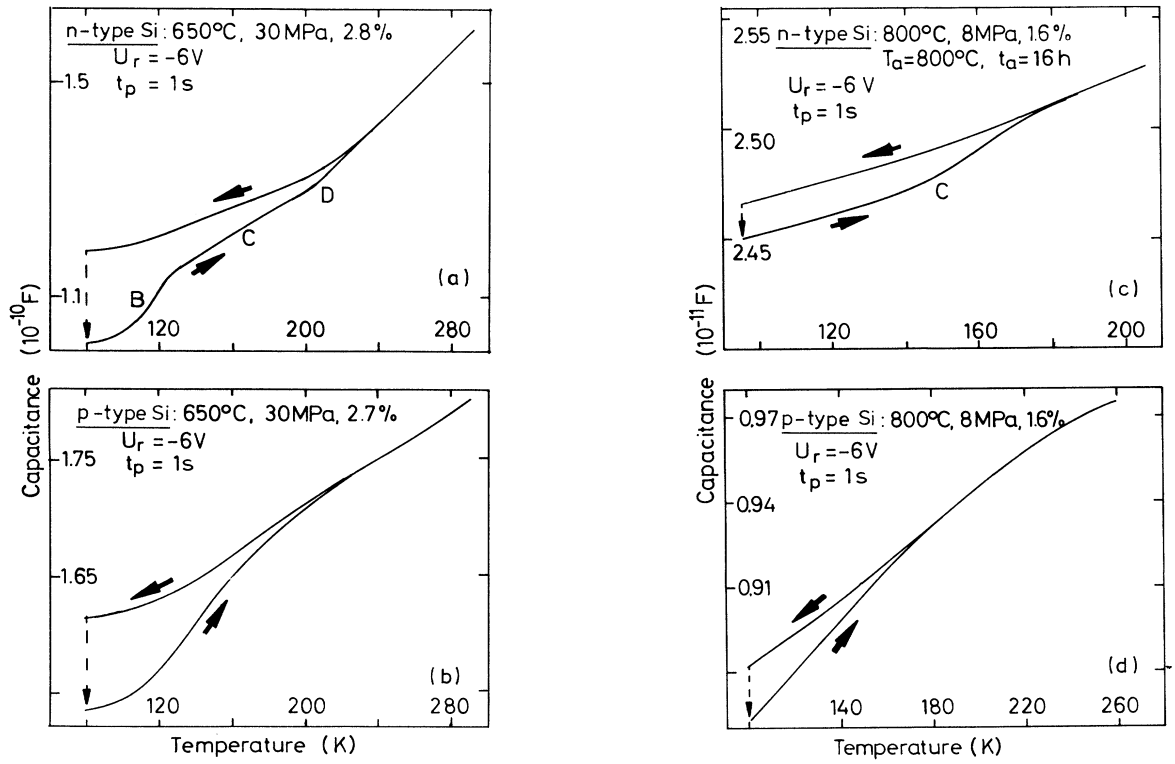

FIG. 2. TSCAP measurements of samples (a) $A2$, (b) $C2$, (c) $F1T$, and (d) $E2$. Arrows mark the direction of temperature scan and the capacitance drop due to the application of a pulse ($U_p = 6$ V) of duration $t_p = 1$ s.

clude that the D-level concentration is small in comparison with the B level.

B. DLTS mesurements of samples deformed at $T_d \leq 650\,^{\circ}C$

In Fig. 3 typical DLTS spectra of samples deformed at $T_d \leq 650\,^{\circ}C$ are shown. Spectra (a) and (c) are well comparable with those published before.[10,12] However, as a result of macroscopic strain ($\epsilon \geq 0.5\%$) during the low-temperature, high-stress deformations similar spectra are created [Figs. 3(b) and 3(d)]: DLTS peaks appear at temperatures comparable to those of Figs. 3(a) and 3(c) but the lines are less well resolved. In the n-type material the B line appears to be broadened; the D line is absent in spectrum (b) in comparison to spectrum (a) and the $C1$-$C2$ line which has been reported to be a line pair[12] is also broadened [cf. Fig. 11(b)]. From comparison of spectra (c) and (d) it is clear that part of the $H.49$ level is absent; the $H.49$ line is known to consist of two contributions.[10]

The filling characteristic of the different traps was observed to be logarithmic for filling times $5\times10^{-7} \leq t_p \leq 10^{-4}$ s (some deviations of the logarithmic filling behavior were detected which were usually caused by superposition of the closely spaced defect levels). With the exception of the D level we generally observed saturation for filling times $t_p \geq 10^{-4}$ s, so that for all other traps concentrations could be determined. They turned out to be in reasonable agreement with the TSCAP data.

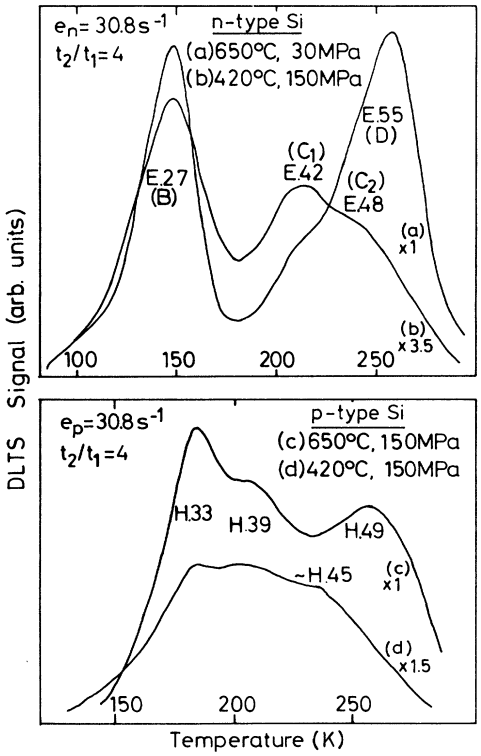

FIG. 3. DLTS measurements of samples (a) $A2$, (b) $A9$, (c) $C4$, and (d) $C6$. $t_1 = 15$ ms, $t_2 = 60$ ms in all cases. $U_1 = -6$ V, and $U_p = 6$ V, and $t_p = 10^{-4}$ s.

The filling behavior of the D level differed from those of the other traps as shown in Fig. 4 where two DLTS spectra detected with different emission rates are compared with the result of the TSCAP measurement of sample $A2$: the reduction of e_n shifts the peak temperature T_0 of the D level from 308 K [4(a)] to 245 K [4(b)] and its amplitude strongly drops in comparison with the other prominent level (B). Its small emission at $\approx$220 K in the TSCAP measurement supports this trend. The defect concentrations in this sample were calculated from Eqs. (4) and (5) and they are plotted in Fig. 5. The strong drop

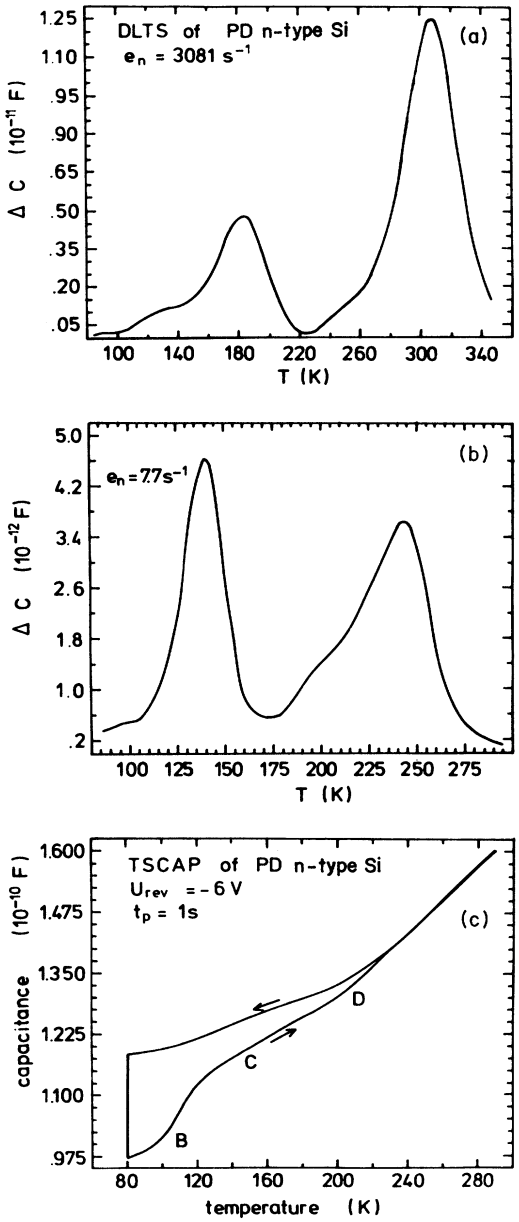

FIG. 4. Dependence of the D-line amplitude on its detection temperature T_0 = (a) 308 K, (b) 245 K, and (c) $\approx$220 K. T_0 is determined by e_n and lowest in the TSCAP measurement. Sample $A2$: Pulse duration in (a) and (b) $t_p = 10^{-4}$ s and in (c) $t_p = 1$ s.

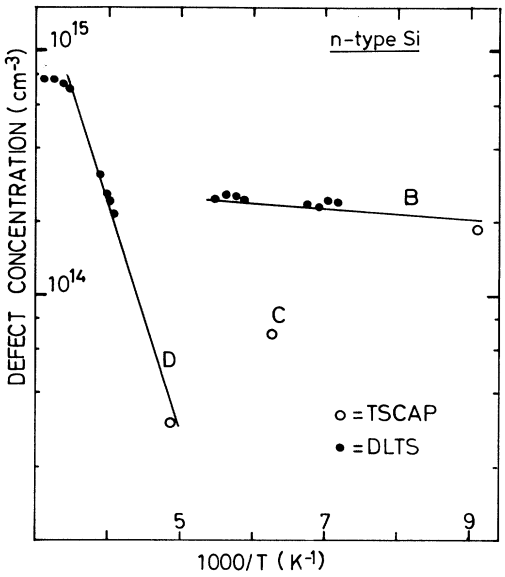

FIG. 5. Temperature dependence of the defect concentration in sample $A2$.

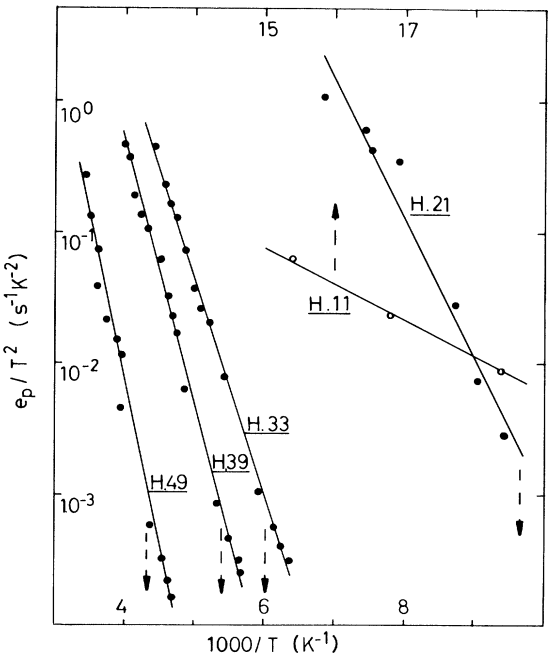

FIG. 7. Determination of apparent activation energies H (in meV) in the p-type sample $C2$. The $H.11$ level refers to the upper abscissa as indicated by the arrows.

of the D level concentration in comparison with the B level is obvious. Since at high temperature the effect vanishes (Fig. 5) and the D level concentration also saturates for $t_p \geq 10^{-4}$ s we always determined its concentration in this temperature range from the DLTS spectrum. This particularity of the D line is not understood and may either be caused by a strong temperature dependence of the capture cross section which would contradict the results of Ref. 12 or more likely it indicates that the defect level is not present at low temperatures which would be in agreement with the TSCAP measurements of Sec. III A and would require a *temperature dependence of the defect structure.* Since the concentration of the D line is not included in the TSCAP data it is additionally listed in Table I.

Apparent activation energies were determined in the usual way[12] and are shown in Figs. 6 and 7. The plots include several levels which were detected cooling the samples down to the freeze-out temperature of the shallow dopants. However, their concentrations were small ($<10^{14}$ cm^{-3}) and they were absent in the low-temeprature, high-stress deformed samples.

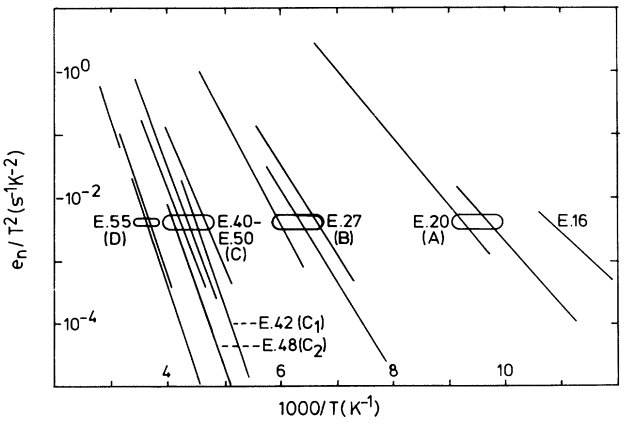

FIG. 6. Determination of apparent activation energies E (in meV) in n-type samples. The plot is taken from Ref. 12 and it indicates typical scattering of the data. $E.16$ was detected in sample $A2$.

In Table III we compare the concentration of the deformation-induced defects as determine from four different measurements (all values are normalized to units of plastic strain ϵ (in %): The first column lists the defect concentrations as determined from TSCAP and DLTS measurements for n- and p-type material (N_t^n, N_t^p) the sum of which is assumed to equal the total density of deformation-induced defects N_t (second column). The third column lists the concentration of ionized shallow impurities as determined from $C(U)$ measurements which is comparable for p- and n-type material as discussed above. However, in the p-doped material this number is uncertain because of the high initial doping (3.2×10^{16} cm^{-3}) and it is better determined from sample $E1$ (Fig. 1). In the n-type material the number of ionized shallow donors can be determined by the drop of the ESR signal of the neutral phosphorous atoms measured before ($P^0=n$) and after deformation ($P_d^0=n_e$) $P^+=P^0-P_d^0$ (Ref. 1) and it is listed in the fourth column. Finally the fifth column lists the spin density of the ESR HT signal of identically deformed intrinsic Si samples.[24,25] This signal was attributed to deformation-induced point defects with no direct relation to the core of dislocations. It can be seen that within deviations up to a factor of 2 (which is not much considering the uncertainties in determining absolute defect concentrations from the different experiments) the total number of deformation-induced defects (N_t) equals the concentration of paramagnetic point de-

TABLE III. Comparison of the defect concentrations determined: second column, DLTS and TSCAP measurements N_t^n, N_t^p; third column, total trap density $N_t = N_t^n + N_t^p$; fourth column, $1/C^2(V)$ measurements (initial doping minus effective doping, for material C this value can only be estimated); fifth column, ESR spectroscopy of the neutral phosphorous signal ($P^+ = P^0 - P_d^0$), sixth column, ESR spectroscopy of deformation-induced point defects. Identically deformed p- and n-type samples are considered (material A and C). Concentrations are given in units of 10^{14} cm^{-3} and are normalized to strain units $[\epsilon] = \%$. The dislocation density is on the level of 10^9 cm^{-2} in our samples.

Sample	N_t^p/ϵ N_t^n/ϵ	N_t/ϵ	$[p-p_e$ (100 K)$]/\epsilon$ $[n-n_e$ (100 K)$]/\epsilon$	P^+/ϵ	ESR/ϵ
$C2, C3$	7.4–11.5		≤ 20		
		9.9–16.5			13.5
$A2$	2.5–5.0		8.9–12.9	11.1	
$C4$	7.0		≤ 20		
		13.5			
$A5$	6.5		12.8	22.0	
$C5$	12.6		≤ 20		
		17.2			
$A8$	4.6		11.1	18.3	
$C6$	7.1		≤ 20		
		10.7			17.0
$A9$	3.6		13.5	24.3	

fects. These defects can capture electrons in n-type material and holes in p-type material from the shallow dopants and thereby change their charge state as shown in Ref. 1. Since they are the dominant deformation-induced defects their concentration equals the reduction of the free-carrier concentration as well as the concentration of ionized phosphorous atoms at low temperature.

This quantitative agreement is schematized for samples

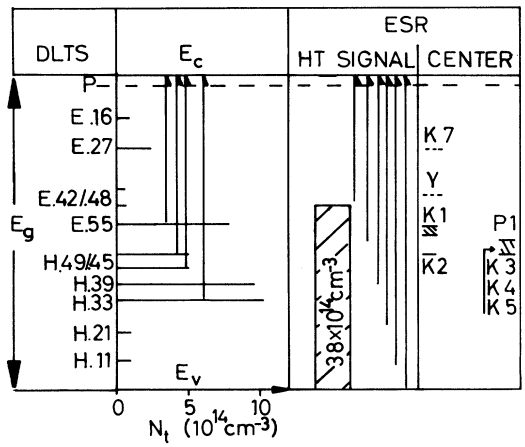

FIG. 8. Comparison of DLTS and ESR measurements. First column: energy levels observed in samples $A2$ and $C2$. Second column: density of the observed traps. Third column: Defect concentration and energy position of the ESR HT signal (Ref. 1). Fourth column: energy position of well-characterized ESR centers. Vertical arrows indicate electron transitions which can be observed in n-type material detecting the ESR signal of neutral phosphorous. For details see text. The paramagnetic centers Si $K1$, Si $K2$, Si Y, and Si $K7$ are dislocation-related defects while Si $K3$, Si $K4$, Si $K5$, and Si $P1$ are point defect clusters (Refs. 1 and 2).

$A2$ and $C2$ in Fig. 8 where the first column lists the detected defect levels and the horizontal lines of the second column indicate their concentrations. From Ref. 1 it is known that in this case the P^0 ESR and the HT ESR signals are small proving that the capture of electrons from the shallow dopants to deep point defects leads to diamagnetic charge states of both types of defects. Their paramagnetic charge state can be reinstalled by photo-ESR performed either on the P^0 or on the HT signal (Ref. 1, Figs. 6 and 7) as indicated by vertical arrows in Fig. 8. Additionally, we show in Fig. 9 that threshold energies of the P^0 photo-ESR signal coincide with the most prominent DLTS levels $E.55$, $H.49$ and $H.45$, $H.39$, and $H.33$. They lie in the range of steep increases of the P^0 photo-ESR signal. However, it should be noted that there is usually a considerable scatter of the apparent activation energies as indicated in Fig. 6. Thus, the association of DLTS levels and photo-ESR threshold energies as done in Fig. 9 suffers from an experimental error of at least 30 meV.

Since the deformation-induced defects form dominant energy levels in the lower half of the band gap and since they can capture electrons as well as holes it is possible to convert n-type to p-type material but p-type material becomes at most highly Ohmic p type by plastic deformation which is in agreement with Hall effect data.[26] However, it cannot be excluded that some deformation-induced donors and acceptors coexist in the deformed samples. The small decrease of the P^0 photo-ESR signal at ≈ 0.8 eV in Fig. 9 could indicate the presence of deformation-induced donors in the n-type sample.

Several proposals were made to relate well-characterized ESR centers with certain DLTS levels[12,27] (Fig. 8, last column). The ESR centers Si $K3$, Si $K4$, Si $K5$ (Ref. 28), and the deformation-induced pentavacancies[29] contribute to the ESR HT signal. Photo-ESR (Refs. 1 and 30) indicates the presence of energy levels of

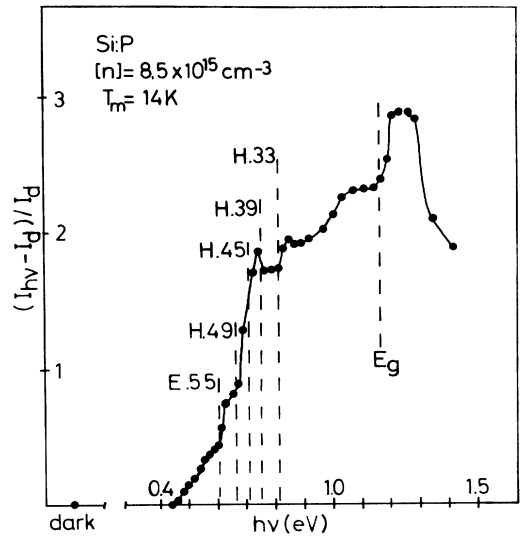

FIG. 9. Coincidence of the dominant DLTS energy levels with threshold energies determined by photo-ESR on the neutral phosphorous atoms (Refs. 1 and 30).

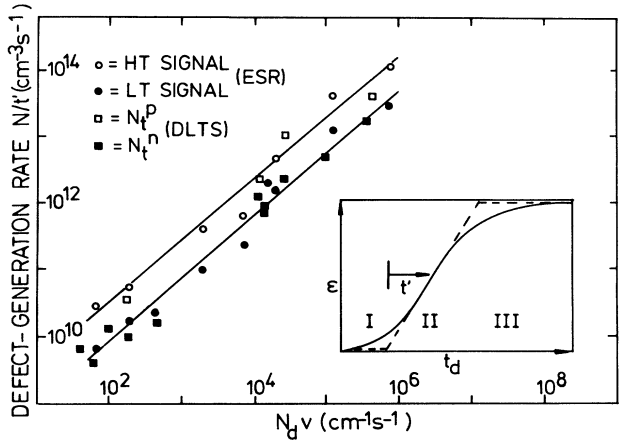

FIG. 10. Dependence of the defect generation rate N/t' in stage II of the creep curve (inset) on the product of dislocation density N_d and dislocation velocity (Ref. 31). The HT and the LT signal were measured by ESR in deformed high-Ohmic crystals whereas $N=N_t^p$ and $N=N_t^n$ are taken from this investigation of p- and n-type silicon. Units: N is in cm^{-3}, t' is in s, v is in cm/s, and N_d is in cm^{-2}.

these defects close to the middle of the band gap as shown in Fig. 8. Other possible energy levels of Si $K3$ to Si $K5$ were detected close to the band edges[30] which are not indicated in Fig. 8 because it is uncertain whether they should be related to the valence- or to the conduction-band edge. At present it cannot be excluded that Si $K3$ to $K5$ contribute to both the $E.55$ and the $H.49$ and $H.45$ levels because the observed reduction of Si $K3$ to Si $K5$ after low-temperature, high-stress deformation which also reduces the $E.55$ and $H.49$ and $H.45$ levels and the absence of defect levels close to the band edges in such samples makes such an identification likely. These defects contribute only with $\approx 20\%$ to the total HT signal which is why most of the other point defects contributing to the HT signal cannot be related to a certain DLTS level. Nevertheless, since the photo-ESR results obtained on the HT signal coincides energetically with the position of the dominant deep-level defects in the lower half of the band gap (Fig. 8) and since these defects appear in comparable concentrations and since ESR indicates that contributions to the HT signal exhibit structural disorder[4,24] which is expected to result in a more continous distribution of energy levels as observed in the lower part of the band gap, the identification of the HT signal with these defect levels is compulsory.

Evidence for the existence of defects in the core of dislocations comes from the structural information of ESR, only.[2] It cannot be given from DLTS experiments. Photo-ESR fixed the energy levels of the Si $K1$-$K2$ center (Ref. 30) shown in Fig. 8. It is proposed to identify one energy level of Si $K1$-$K2$ with the $E.55$ level[12] which in this case would coincide with possible contributions of Si $K3$–$K5$. The dependence of the $E.55$ level formation on T_d agrees with the observation that the formation of the ESR center Si $K1$ decreases also with decreasing T_d^4. It was concluded that Si $K1$ includes an impurity.[2] One energy level of Si $K2$ is very close to the $H.49$ and $H.45$ level but this identification also suffers from possible additional contributions of energy levels from point defects.

It was also proposed to identify the C level ($E.42$ and $E.48$) with the ESR center Si Y (Refs. 12 and 27) because both the ESR resonance and the C level are composed of at least two contributions[4,12] and thermally they are the most stable defects [Fig. 11(b)].[31] In the previous paper[1] it was shown that its paramagnetic and probably neutral charge state (which follows from a model which proposes to identify Si Y with threefold-coordinated vacancies in the core of screw dislocations which may incorporate oxygen to some extent[12]) can hardly be changed. If so, one would expect that in the weak n-doping range only about 10–15 % (this is the accuracy of the ESR investigation of Ref. 1) of the total defect concentration ($\approx 1.5\times 10^{14}$ $cm^{-3}=10\%$ of the value from Fig. 12 in Ref. 1) could capture electrons and, therefore, could be detected by DLTS. This is indeed close to the concentration of the C level given in Fig. 5.

An energy level of Si $K7$ was tentatively identified with the B line.[12] However, Si $K7$ turned out to be one example of a class of defects found in deformed n-type Si which are electric-dipole spin resonances exhibiting distinctly different g tensors.[1] It is at present not clear whether one of them correlates with the B line.

The paramagnetic defects measured in highly Ohmic crystals by ESR and the deep traps detectable by DLTS in doped crystals exhibit the same generation law as shown in Fig. 10 taken from Ref. 31. It can be seen that the defect density N (no matter whether it is determined by DLTS $N=N_t^{p,n}$ or ESR $N=N_{\mathrm{HT,LT}}$) is proportional to $t'(N_d v)^k$ with N_d equal to dislocation density, v equal to dislocation velocity, and t' equal to deformation time during stage II of the creep curve (Fig. 10, inset). From linear regressions the exponent k turns out to be very close to one in all cases ($0.92 \le k \le 0.95$). A description

with $k=1$ suggests that the defect formation is proportional to the distance $s=vt'$ moved by the dislocations[31] and that dominant contributions to the defect formation come from stage II of the creep curve. Even though the relation is not fully understood[31] it stresses the identity of the defects measured by ESR and DLTS and it suggests that point defects contributing to the HT signal give rise to energy levels in the lower half of the band gap whereas the energy levels of dislocation related defects can be found in its middle and its upper part. This similarity allowed for a choice of the deformation parameters such that the defect density is still smaller than the density of chemical dopants but large enough to be able to perform ESR experiments and this is also why the trap concentrations are rather similar in the different samples. However, the scattering of the data does not allow for a doubtless specification of a model or for a further specification of functional dependences such as on the dislocation density or dislocation morphology which strongly depends on the deformation temperature and the resolved shear stress.[32] In this connection it is noteworthy that the homogeneity of the deformation and the formation of dislocation wall structures was observed to be different in samples deformed with the same stress ($\tau=150$ MPa) but at different temperatures (650 °C and 420 °C).[33]

C. High-temperature deformations and hydrogen-induced defect reduction

In Fig. 11 the DLTS spectra of high-temperature deformed as well as of deformed and annealed samples are shown. Identical spectra were observed in samples deformed in an argon gas ambient with the exception of the DLTS signal detectable below 120 K in the p-type material. However, it could not be clarified whether the additional signal is caused by the presence of hydrogen.

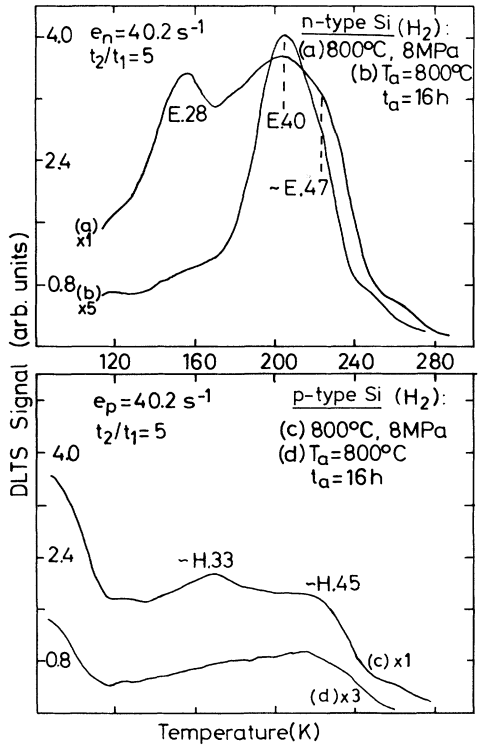

FIG. 11. DLTS mesurements of samples (*a*) *F2*, (*b*) *F2T*, (*c*) *E3*, and (*d*) *E3T*. $t_1=10$ ms, $t_2=50$ ms in all cases. $U_1=-6$ V, $U_p=6$ V, and $t_p=10^{-4}$ s.

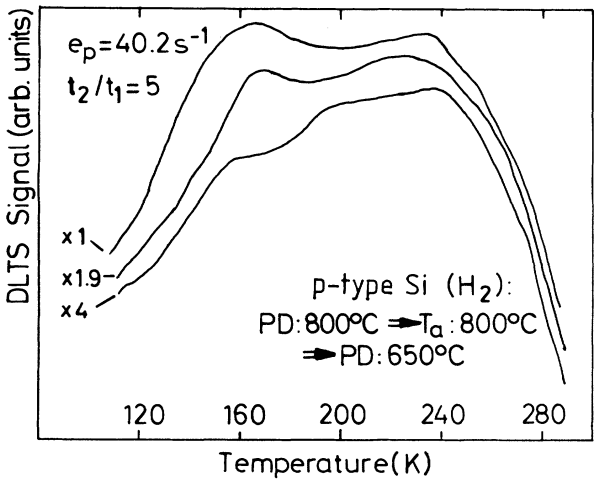

FIG. 12. DLTS spectra of the three step deformed sample *C7*. The spectra are taken at different distances from the initial sample surface (Table IV). Close to the surface only ≈25% of the defect density measured in the center of the sample is detectable as indicated by the amplification factor.

From Fig. 11 and Table II it can be seen that after high-temperature deformation there are still residual contributions present which are known from the low-temperature deformed crystals. The annealing reduced the spectra to the *C* line in the n-type material and to a broad band in the p-type material. In the annealed samples the total trap concentration is on the level of 2×10^{13} cm^{-3} and in such samples electrical properties of dislocations could be studied best.[1,31]

A three step deformation in a molecular hydrogen ambient performed with the intent to introduce deep-level defects during the second deformation (Table II, sample *C7*) can be used to cause a reduction of the deep defect concentration.[5] Indeed, we observed that in sample *C7* the defect density can strongly be reduced (Fig. 12) even though the reduction was more effective in regions close to the initial sample surface than in its center (Table IV). This hydrogen-induced defect reduction was also observed by ESR detection of the HT signal[5] and it again stresses the correlation of the HT signal with defect levels in the lower part of the band gap.

TABLE IV. Defect concentration as determined by TSCAP measurements of the hydrogen treated sample *C7*. *d* is the mean distance of the Schottky contact to the closest initial surface of the sample.

N_t^p (10^{14} cm^{-3})	Distance *d* (mm)
30.7	1.9±0.4
17.0	1.0±0.4
8.0	0.5±0.4

D. Level broadening and inhomogeneity

The most striking feature of the DLTS spectra considered here is the observation that with increasing deformation stress and reduced deformation temperature the width of the B line [Fig. 3, spectra (a) and (b)] as well as of the C line [Fig. 3 spectrum (b) and Fig. 11 spectrum (b)] increases. Also, the degeneration of the DLTS spectra in high-stress, low-temperature deformed p-type samples to a broad band [Fig. 5, spectra (c) and (d)] indicates this trend.

Omling *et al.*[12] attempted to explain the line width of the B and the D line in a sample deformed at 650 °C with $\tau = 30$ MPa (sample $A2$) in terms of a model which introduces a Gaussian broadening of the energy levels with a mean value at E_t and a broadening parameter δ [root-mean-square value of the distribution; Eq. (5)]. More generally, Das, Singh, and Lang[23] used the broadening parameter to define weak and strong disorder in the crystals (weak disorders: $s = \delta/E_t < 0.1$ and $b = \delta/kT < 1$; strong disorder $s > 0.1$ and $b > 1$). The main difficulty in the application of Eq. (5) to our spectra is that with the exception of the B line (Fig. 3) isolated defect levels can hardly be detected. The published value $\delta = 16$ meV (Ref. 12) for the D line suffers from the fact that the D line is strongly distorted in those cases where it appears to be isolated. This can be seen from Fig. 13 where it is shown that the spectrum is strongly distorted depending on the applied pulse amplitude U_p. The distortion is most pronounced if U_p exceeds the reverse bias $U_p \geq U_r$ [in Fig. 13, curve (b) the total forward potential is $\approx +1.2$ V; $U_0 \approx -0.8$ V]. A spectrum like the one of Fig. 3 curve (a) can easily be recorded by use of other pulse voltages. The distortion sharpens the D line much stronger than the B line. The effect may either be caused by resistances in series with the junction but more likely we think that it is due to minority carrier emission in particular because a similar effect was recently observed in plastically deformed n-type GaAs with negligible junction resistance.[34]

In Fig. 14 typical DLTS spectra together with fitting points calculated from Eq. (5) are shown: In the case of the B line a baseline correction was necessary because of distortions coming from the C line which has a wing extending towards low temperature (Fig. 11).[11,15] This baseline correction underestimates the true linewidth, in particular, in the high-stress deformed samples. As to the D line, only its high-temperature wing was used to determine δ and only spectra recorded with $U_p < |U_r|$ were analyzed (Fig. 13). This fitting procedure revealed the C_2 line which up to now could not be observed in samples deformed at 650 °C with $\tau = 30$ MPa. It can be seen that in this case we found $\delta = 22.5$ meV for both lines which suggests that the broadening is no specific property of a certain defect. In sample $E1$ we also could observe an isolated line probably because of electron emission in the strongly compensated p-type sample. We, therefore, consider the value $\delta = 15$ meV obtained for $H.29$ less reliable. However, this proves that the defects in the lower half of the band gap exhibit a similar line broadening.

In Fig. 15 we plotted δ obtained from the different deformed samples versus the external stress σ applied during the deformation procedure. (The load was not removed during the cooling procedure following the deformation.) It can be seen that the width of the B line increases with 21.5 meV per GPa external stress. Reliable values for the D line can only be given for low-stress deformed samples because the D line vanishes with increas-

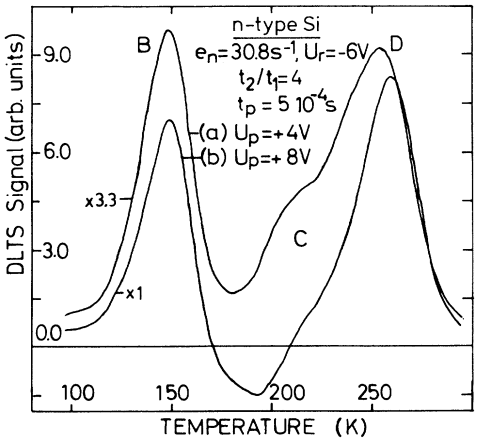

FIG. 13. Dependence of the DLTS spectrum on the chosen pulse voltage. Sample $A2$.

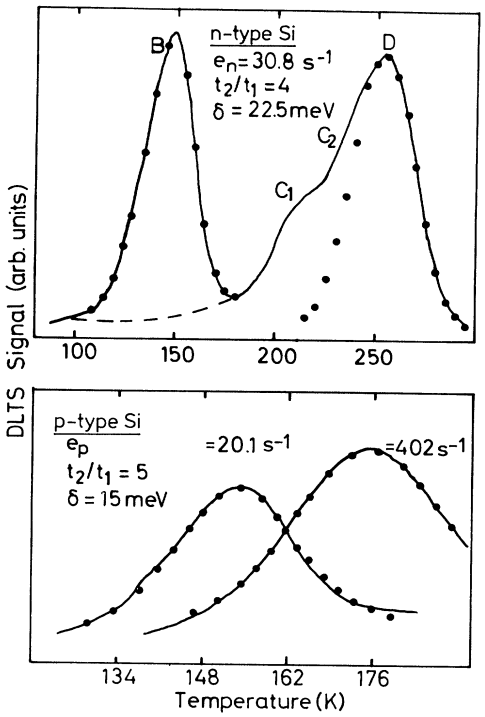

FIG. 14. Simulation of the DLTS lines B and D in n-type material and the $H.29$ level in p-type material by Eq. (5). Samples $A2$ and $E1$. The dashed line indicates the baseline correction for the B line. Simulation parameters: $E.28$ (B line), $A = 5\times10^6$ s^{-1}K^{-2}; $t_1 = 15$ ms; $t_2 = 60$ ms. $E.55$ (D line), $A = 3\times10^7$ s^{-1}K^{-2}; $t_1 = 15$ ms; $t_2 = 60$ ms. $H.29$ (1), $A = 4\times10^6$ s^{-1}K^{-2}; $t_1 = 20$ ms; $t_2 = 100$ ms. $H.29$ (2), $A = 4\times10^6$ s^{-1}K^{-2}; $t_1 = 1$ ms; $t_2 = 5$ ms.

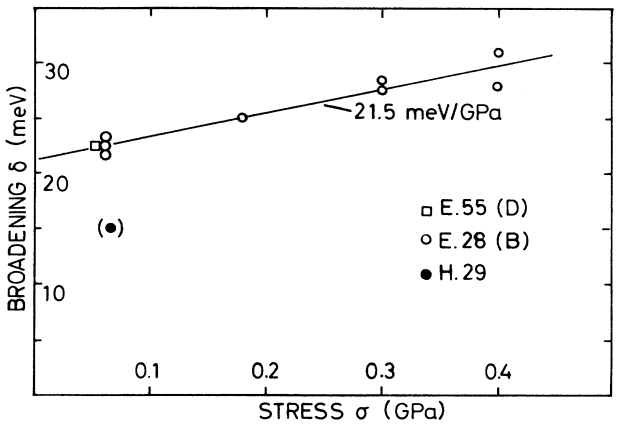

FIG. 15. Dependence of the broadening parameter δ on the stress applied during the deformation. Samples: $A2$, $A3$, $A6$, $A7$, $A8$, $A9$, $A10$ (two different slices), and $E1$.

ing deformation stress at low deformation temperature and in high-temperature, high-stress deformed samples the distortion shown in Fig. 13 was even more pronounced.

If we apply the classification suggested by Das, Singh, and Lang[23] (Table V) it can be seen that the DLTS linewidths of the deformed crystals cover the region from weak to strong disorder while DLTS measurements of grain boundaries or of a-Si:H (as far as they are available) fall into the region of strong disorder. Since this result suggests a systematic increase of disorder from deformed to amorphous silicon we discuss our results on the background of possible contributions to disorder introduced by the deformation of the crystals.

Local strain (due to the presence of dislocations) changes bond angles and bond lengths and introduces states split off from the band edges or tail states.[35] Since our value of 21.5 meV/GPa is very close to the pressure derivative of the conduction band ($\approx$24 meV/GPa) (Ref. 36) the result suggests that the observed broadening should not be exclusively attributed to a broadening of the DLTS level itself but partly results from the formation of split off or tail states. This suggestion finds support from the facts that the formation of such states increases at least from polycrystalline to amorphous silicon[35] and that in deformed crystals states close to the band edges were observed by microwave conductivity measurements which also depend on the stress applied during the deformation.[37] As to the depth of the deformation-induced split-off states it was estimated to $E_t \leq 80$ meV.[37] Since the full width at half maximum of the Gaussian broadening of the energy levels in our case is related to the broadening parameter δ by $2\delta(2\ln 2)^{1/2}$, it varies from 47 to 71 meV for $\delta = 20$–30 meV (B level). These values are well comparable with the results obtained from conductivity measurements.

TABLE V. Characterization of the DLTS line broadening in different materials according to the suggestion of Ref. 23 in terms of weak disorder ($\delta/kT < 1$ and $\delta/E_0 < 0.1$) and of strong disorder ($\delta/kT > 1$ and $\delta/E_0 > 0.1$).

Material	δ/kT	δ/E_0	Ref.
Deformed Si	1.5–2.3	0.07–0.11	This work
Grain boundary	$\approx$2.8	$\approx$0.13	From Fig. 7(a) (Ref. 40)
a-Si:H	$\approx$6	$\approx$0.2	Ref. 23

The surprising result that the DLTS linewidth reflects the external stress applied during the deformation procedure is similar to ESR investigations of deformation-induced pentavacancies[29] and of Si $K1$ (Ref. 2) where a dependence of elastic defect properties on the external stress applied during the deformation was also observed. It may be related to the fact that during the deformation procedure both the internal and the external stresses determine the total stress the defects are subject to. During the DLTS (or the ESR) investigations the external load is removed and this may be why we observe frozen-in strain components which from their magnitude reflect the external stress but they would be caused by its absence.

Level broadening may also be caused by fluctuations of the potential energy occurring between different sites of randomly distributed charged defects. Morgan[38] and Stern[39] succeeded in relating the broadening parameter δ of a Gaussian distribution of Coulomb potentials to the screening length L by

$$\delta = (e^2/\epsilon\epsilon_0)[(N_a + N_d)L/8\pi]^{1/2} \tag{6}$$

where ϵ is the dielectric constant, ϵ_0 is the permitivity, and N_d, N_a being the number of ionized donors or acceptors, respectively.

In the low-temperature limit with the assumption that all donors and acceptors are ionized the screening length L for n-type material is given by[39]

$$L^2 = \epsilon\epsilon_0 kT/e^2 N_a(1-K_n) \tag{7}$$

(in p-type material N_d replaces N_a and K_p replaces K_n) from which it can directly be seen that the ionization of impurities and the compensation determine the broadening parameter δ.

Unfortunately, the charge state of the deformation-induced defects is unknown and their distribution is inhomogeneous with respect to the shallow dopants.[1] But K_n or K_p must be large in our samples (Fig. 1). Therefore, only rough estimations can be given: If we take the results of sample $A2$ where after the deformation with ϵ equal to 2.8% about 0.7×10^{16} cm^{-3} ionized shallow donors and deep defects exist on the average (Table III) and if we consider the results of Ref. 1 which state that the defects are inhomogeneously distributed with respect to the shallow dopants one could expect local defect concentrations N_l in the range 10^{16}–10^{17} cm^{-3}. If we further approximate the screening length by the mean distance between the charged ions ($N_l = N_a + N_d$) $L^* = (3/4N_l\pi)^{1/3}$ as suggested by Morgan[38] we may roughly estimate δ from (6). The result is shown in Fig. 16 and we find that in the relevant defect concentration range contributions up to 10 meV to the level broadening can be expected which naturally would contribute to the

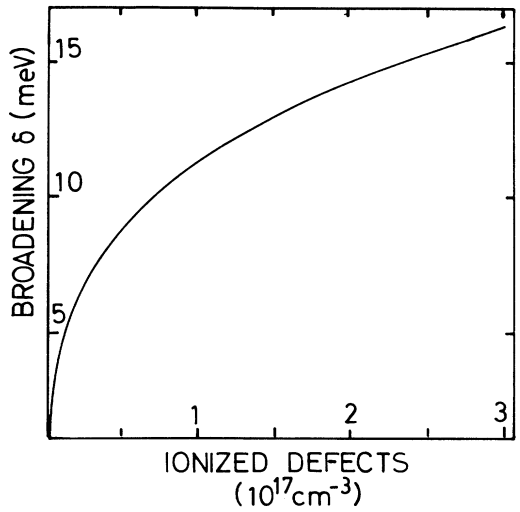

FIG. 16. Estimated dependence of the broadening parameter δ on the total concentration of ionized defects [Eq. (6)].

level broadening for $\sigma = 0$ MPa in Fig. 15.

Finally it is likely that Eq. (5) is oversimplified because it ignores a scatter of the capture cross section.[23] It is known to scatter in the case of DLTS measurements on grain boundaries[40] and Münzberg, Palm, and Schulz[41] recently showed that compensation, which in case of our experiments has been shown to be large, probably influence the capture of charged carriers.

Thus, the results outlined in this and the preceding paper[1] indicate substantial local distortions of the energy gap caused by local shifts of the band edges (Ref. 1, Figs. 14 and 15) and in addition by the formation of split-off states or band tails which seem to be at least partly related to the broadening parameter δ. This situation is very similar to what has been discussed for grain boundaries in polycrystalline material by Madenach and Werner[42] who applied noise spectroscopy to bicrystals and to multicrystalline silicon: at grain boundaries they determined a shift of the band edge (mean barrier height) around 300 meV and a Gaussian potential fluctuation at the band edges with a standard deviation σ' up to 70 meV. In the case of deformed crystals the local shift of the band edges depends on the local compensation. It can reach values as large as 450 meV (Ref. 1) and it is well comparable with the barrier heights of grain boundaries. If we attribute the broadening parameter δ exclusively to the potential fluctuations characterized by the standard deviation σ', our values $\delta = \sigma' \leq 30$ meV are considerably smaller than in the case of grain boundaries. It is, therefore, tempting to ascribe the continous distribution of states within the band gap at grain boundaries[42] to the large value of $\delta = \sigma' = 70$ meV and in the case of DLTS measurements a continuous defect spectrum could be expected in contrast to our samples where individual traps are broadened but still resolvable.

It is worth it to investigate the influence of the considered broadening mechanisms on the filling behavior of traps which was not attempted in this study. The rather similar and partly logarithmic filling behavior of all deformation-induced defects no matter whether they are located in the core of dislocations or not indicates that the logarithmic filling behavior is no specific feature of defects in the core of dislocations as often argued but it may indicate the presence of dislocations or compensation in the crystals.

IV. CONCLUSION

Quantitative and qualitative agreement is achieved determining the concentration of deformation-induced defects by DLTS and ESR. It is shown that point defects with no structural relation to dislocations dominate the electrical properties of deformed crystals by introducing deep-level defects mostly in the lower half of the band gap. Defects in the core of dislocations most likely produce midgap levels and levels in the upper part of the band gap. These two type of defects can be distinguished from structural informations of ESR spectroscopy, only; the logarithmic filling behavior does not necessarily imply a location of the defects on dislocations. Most of the defects are amphoteric and act donorlike in *p*-type material and acceptorlike in *n*-type silicon.

With the possible exception of the *C* level, if attributed to the ESR center Si *Y*, it is proposed that the trapping processes are limited by the inhomogeneous distribution of the deep defects with respect to the shallow dopants which may locally compensate the crystals even if their average concentration is less than the initial doping.

The DLTS levels are found to be broadened as a result of the inhomogeneous introduction of dislocations and point defects which are expected to fluctuate on the same scale than the dislocation density does (0.5–5 μm). The level broadening could be described by a broadening parameter δ which accounts for the disorder in the crystal. From its value (20–30 meV) it covers the transition region from weak to strong disorder. In *n*-type material δ depends on the applied deformation stress by 21.5 meV/GPa and the value is close to the pressure derivative of the conduction-band edge. This suggests that part of the energy distribution should be attributed to fluctuations at the band edge. The full width at half maximum of the energy distribution reaches 70 meV and we consider strain effects which result from the applied load during the deformation, compensation, and scatter of the capture cross sections likely to contribute to the broadening.

ACKNOWLEDGMENTS

The authors acknowledge experimental support in running the DLTS spectrometer by W. Tseng. Measurements down to 20 K were done at the Center of Advanced Materials, Lawrence Berkeley Laboratory, with kind help of D. D. Nolte and E. E. Haller. Control samples were investigated at Hewlett Packard, Palo Alto. Details of DLTS spectroscopy and the experimental results were discussed with P. Omling and H. Alexander, respectively. The Deutsche Forschungsgemeinschaft as well as the Director, Office of Basic Energy Research, Office of Basic Energy Sciences, Materials Science Division of the U.S. Department of Energy, under Contract No. DE-AC03-76SF00098, supported the project.

[1]C. Kisielowski, J. Palm, B. Bollig, and H. Alexander, preceding paper, Phys. Rev. B **44**, 1609 (1991).
[2]C. Kisielowski-Kemmerich, Phys. Status Solidi B **161**, 111, (1990).
[3]R. Labusch and W. Schröter, in *Dislocations in Solids,* edited by F. R. N. Nabarro (North-Holland, Amsterdam, 1980), Vol. 5, p. 127.
[4]C. Kisielowski-Kemmerich and H. Alexander, Fiz. Tverd. Tela (Leningrad) **31**, 254 (1989) [Sov. Phys.—Solid State **31**, 864 (1989)].
[5]U. Voermanns, C. Kisielowski-Kemmerich, and H. Alexander, in *Science and Technology of Defect Control in Semiconductors,* edited by K. Sumino (Elsevier, Amsterdam, 1990), p. 1357.
[6]R. H. Glaenzer and A. G. Jordan, Solid-State Electron. **12**, 247 (1969).
[7]L. C. Kimerling and J. R. Patel, Appl. Phys. Lett. **34**, 73 (1979).
[8]W. Szielko, O. Breitenstein, and R. Pickenheim, Cryst. Res. Technol. **16**, 197 (1981).
[9]B. Pohoryles, Phys. Status Solidi A **67**, K75 (1981).
[10]V. V. Kveder, Yu. A. Osipyan, W. Schröter, and G. Zoth, Phys. Status Solidi A **72**, 701 (1982).
[11]W. Schröter and M. Seibt, J. Phys. (Paris) Colloq. **44**, C4-329 (1983).
[12]P. Omling, E. R. Weber, L. Montelius, H. Alexander, and J. Michel, Phys. Rev. B **32**, 6571 (1985).
[13]H. Ono and K. Sumino, J. Appl. Phys. **57**, 287 (1985).
[14]N. A. Yarkin and O. V. Feklisova, in *Defects in Crystals,* edited by E. Mizera (World Scientific, Singapore, 1988), p. 366.
[15]W. Schröter, I. Queisser, and J. Kronewitz, in *Structure and Properties of Dislocation in Semiconductors 1989,* edited by S. G. Roberts, D. B. Holt, and P. R. Wilshaw, IOP Conf. Proc. No. 104 (Institute of Physics and Physical Society, London, 1989), p. 75.
[16]C. T. Sah, W. W. Chan, H. S. Fu, and J. W. Walker, Appl. Phys. Lett. **20**, 193 (1972).
[17]J. Bourgoin and M. Lannoo, in *Point Defects in Semiconductors II,* Springer Series in Solid-State Sciences Vol. 35 (Springer, New York, 1983), p. 179.
[18]The system was developed by W. Tseng.
[19]D. V. Lang, J. Appl. Phys. **45**, 3023 (1974).
[20]The system works with a Boonton bridge and a Miller correlator. Samples were cooled by compression of helium.
[21]J. Bourgoin and M. Lannoo, in Ref. 17, p. 167.
[22]P. Omling, L. Samuelson, and H. G. Grimmeiss, J. Appl. Phys. **54**, 5117 (1983).
[23]A. Das, V. A. Singh, and D. V. Lang, Semicond. Sci. Technol. **3**, 1177 (1988).
[24]C. Kisielowski-Kemmerich, G. Weber, and H. Alexander, J. Electron. Mater. **14A**, 387 (1985).
[25]C. Kisielowski-Kemmerich, Ph.D. thesis, Universität Köln, 1985.
[26]V. A. Grazhulis, V. V. Kveder, and V. Yu. Mukhina, Phys. Status Solidi A **43**, 407 (1977).
[27]E. R. Weber, P. Omling, C. Kisielowski-Kemmerich, and H. Alexander, Izv. Akad. Nauk USSR Ser. Fiz. **51**, 664, 1987 [Bull. Acad. Sci. USSR, Phys. Ser. **51**, 18 (1987)].
[28]E. Weber and H. Alexander, in *Radiation Effects in Semiconductors 1976,* edited by N. B. Urli and J. W. Corbett, IOP Conf. Proc. No. 31 (Institute of Physics and Physical Society, London, 1977), p. 266.
[29]M. Brohl, C. Kisielowski-Kemmerich, and H. Alexander, Appl. Phys. Lett. **50**, 1733 (1987).
[30]R. Erdmann and H. Alexander, Phys. Status Solidi A **55**, 251 (1979); R. Erdmann, Ph.D. thesis, Universität Köln, 1979.
[31]C. Kisielowski-Kemmerich and H. Alexander, in *Defects in Crystals,* edited by E. Mizera (World Scientific, Singapore, 1988), p. 270.
[32]H. Alexander, in Ref. 3, Vol. 5, p. 113.
[33]E. Heister (unpublished).
[34]A. Fanelsa, Diploma thesis, Universität Köln, 1990.
[35]J. H. Werner, in Ref. 15, p. 63.
[36]Landolt-Börnstein, Vol. 22b, edited by O. Madelung and M. Schultz (Springer, Berlin, 1989), p. 310.
[37]M. Brohl and H. Alexander, in Ref. 35, p. 163.
[38]T. N. Morgan, Phys. Rev. **139**, A343 (1965).
[39]F. Stern, Phys. Rev. B **9**, 4597 (1974).
[40]A. Broniatowski, Phys. Rev. B **36**, 5895 (1987).
[41]M. Münzberg, H. Palm, and M. Schultz, Appl. Phys. A **50**, 255 (1990).
[42]A. J. Madench and J. H. Werner, Phys. Rev. B **38**, 13 150 (1988).